Dresselhaus spin-orbit interaction in the *p*-AlGaAs/GaAs/AlGaAs structure with a square quantum well: Surface acoustic wave study

I. L. Drichko,[1] I. Yu. Smirnov,[1] A. V. Suslov,[2] K. W. Baldwin,[3] L. N. Pfeiffer,[3] and K. W. West[3]
[1]*Ioffe Physical-Technical Institute, Russian Academy of Sciences, St. Petersburg 194021, Russia*
[2]*National High Magnetic Field Laboratory, Tallahassee, Florida 32310, USA*
[3]*Department of Electrical Engineering, Princeton University, Princeton, New Jersey 08544, USA*

(Received 16 April 2021; revised 27 August 2021; accepted 28 September 2021; published 6 October 2021)

The effect of spin-orbit interaction was studied in a high-quality *p*-AlGaAs/GaAs/AlGaAs structure with a square quantum well using acoustic methods. The structure grown on a GaAs (100) substrate was symmetrically doped with carbon on both sides of the quantum well. Shubnikov–de Haas–type oscillations of the ac conductance of two-dimensional holes were measured. At a low magnetic field $B < 2$ T, conductance oscillations undergo beating induced by a spin-orbit interaction. Analysis of the beating character made it possible to separate the conductance contributions from the two heavy-hole subbands split by the spin-orbit interaction. For each of the subbands the values of the effective masses and quantum relaxation times were determined, and then the energy of the spin-orbit interaction was obtained. The quantum well profile, as well as the small magnitude of the spin-orbit interaction, allowed us to conclude that the spin-orbit splitting is governed by the Dresselhaus mechanism.

DOI: 10.1103/PhysRevB.104.155302

I. INTRODUCTION

An electron (hole) system in low external magnetic fields or in the absence of a magnetic field is usually considered a spin degenerate one. However, in some cases, namely, when a spin-orbit interaction exists in the system, it turns out that the spin degeneracy can be lifted even in the absence of a magnetic field. Two causes of the lifting of the spin degeneracy are known. One of them is the crystal structure of the material under study: the lack of spatial inversion symmetry, which is typical, for example, in systems with the zinc-blende crystal structure ($A^{III}B^{V}$) [1]. The second cause is the structural inversion asymmetry of the quantum well [2,3]. The spin-orbit interaction is commonly studied experimentally by measuring the Shubnikov–de Haas (SdH) oscillations. Since the spin-orbit interaction induces the formation of two subbands with different spin directions at each wave vector and different concentrations and because the magnitude of the spin-orbit splitting is small, in transport experiments this effect manifests itself in the beating of the oscillations. By now, beating of the Shubnikov–de Haas oscillations has been observed and extensively studied in many electronic two-dimensional systems. These are InAs/GaSb, InAs/AlSb [4,5], $Ga_xIn_{1-x}As$/InP [6–8], $Al_xGa_{1-x}N$/GaN [9], $In_{0.53}Ga_{0.47}As/In_{0.52}Al_{0.48}As$ [10–12], and HgTe [13–16]. The objects of the studies in the papers referred to above were mainly heterostructures or one-side-doped quantum wells. As for two-dimensional hole systems, aside from work [17] performed on the InGaAs/GaAs heterostructure, the experiments were carried out mainly on *p*-GaAs/AlGaAs samples [18–23]. In these works, the objects under study were also, for the most part, heterostructures or one-side-doped quantum wells. Moreover, two-dimensional structures were formed on GaAs substrates with the (311)A orientation, and the dopants were either Be or Si. Relatively recently, high-quality *p*-GaAs/AlGaAs structures were grown on GaAs substrates oriented along (100) and doped with carbon. The mobility in these structures reached a value exceeding 10^6 cm^2/V s [24]. In these systems studies of the spin-orbit interaction have already been performed in [25–28]. In both the heterostructure investigated in Ref. [25] and the one-side doped quantum well studied in Ref. [26], the influence of the spin-orbit interaction on SdH oscillations was clearly seen. However, in the symmetric quantum well with high mobility and a low concentration studied in [27] no spin-orbit interaction was experimentally observed. In [28], in a symmetrically doped quantum well ($p = 2.2\times10^{11}$ cm^{-2}, $\mu = 0.7\times10^6$ cm^2/V s at 300 mK), beating of the SdH oscillations was observed. However, its Fourier spectrum peak splitting, which is specific to the existence of two spin-split subbands, was too weak and could not be analyzed to obtain such characteristics as the effective mass in each subband.

In this work, we investigate the effect of the spin-orbit interaction on the ac conductance of holes in a 17 nm wide quantum well symmetrically doped with C. The structure was grown on the (100) GaAs substrate. The measurements were carried out using the surface acoustic waves (SAW) technique in the frequency range of 30–300 MHz in magnetic fields up to 18 T, at temperatures of 20–300 mK in a linear regime in the wave power, and at $T = 20$ mK at various SAW intensities.

II. SAMPLE PARAMETERS AND METHOD

The high-quality samples were multilayer (29 layers) structures grown on a GaAs (100) substrate. The single quantum

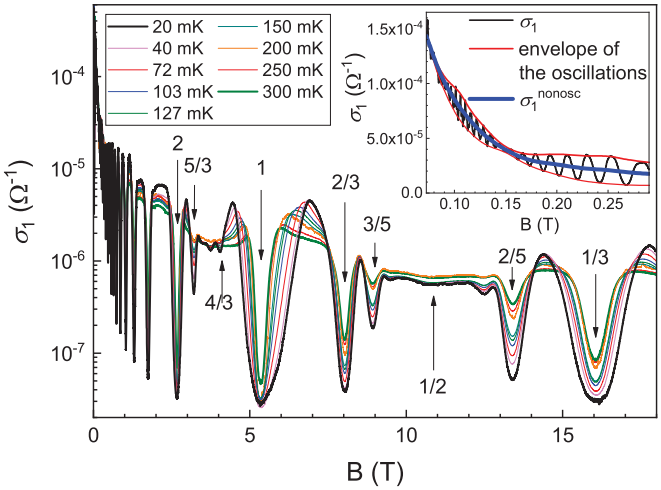

FIG. 1. Magnetic field dependence of σ_1 at different temperatures and at $f = 85$ MHz. The arrows indicate the filling factors ν. Inset: expanded view of σ_1 for magnetic fields below 0.3 T at 20 mK with the oscillation envelope and its average, i.e., the nonoscillating background.

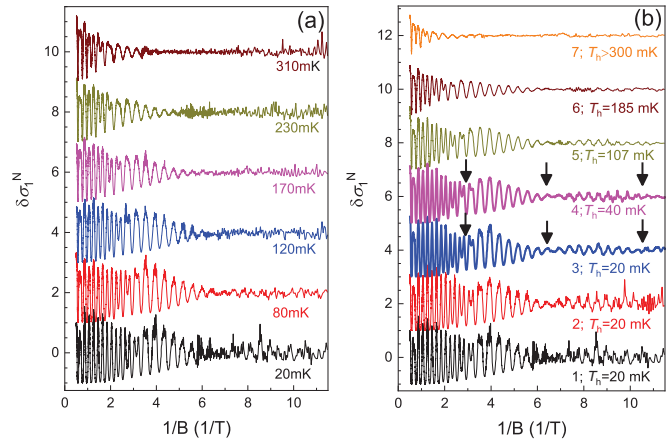

FIG. 2. Dependences of $\delta\sigma_1^N$ on $1/B$ (a) as varied with temperature at a SAW intensity of 6×10^{-10} W/cm and (b) as varied with the SAW powers at $T = 20$ mK: (1) 6×10^{-10} W/cm, (2) 1.9×10^{-9} W/cm, (3) 6×10^{-9} W/cm, (4) 1.9×10^{-8} W/cm, (5) 6×10^{-8} W/cm, (6) 1.9×10^{-7} W/cm, and (7) 1.9×10^{-6} W/cm. $f = 30$ MHz. The hole temperature T_h is shown for each of the curves. See the definition of T_h in the text and in Fig. 3. Traces are offset vertically for clarity. Arrows indicate the oscillations' beating nodes.

well in the structure is a 17 nm wide GaAs layer. It is bounded on both sides by 100 nm layers of $Al_{0.24}Ga_{0.76}As$ barrier material acting as symmetrical undoped setbacks from the carbon δ-doped layers on each side. Formed in such a way, the quantum well is a square, highly symmetrical one. The quantum well is located at a depth of 210 nm below the surface of the sample. It has hole concentration $p = 1.2 \times 10^{11}$ cm^{-2} and mobility $\mu = 1.8 \times 10^6$ cm^2/V s at 300 mK.

In our studies we utilize the surface acoustic wave technique. In these probeless acoustic experiments a SAW propagates along a surface of a piezoelectric lithium niobate delay line, on either edge of which interdigital transducers are placed to excite and detect the wave. The structure under study is pinned down on the surface of the $LiNbO_3$ crystal by means of springs. The electric field accompanying the SAW penetrates into the two-dimensional (2D) channel. This ac field induces electrical currents in the 2D hole gas (2DHG), which, in turn, cause Joule losses. As a result of the coupling of the SAW electric field with charge carriers in the quantum well, the SAW attenuation Γ and its velocity shift $\Delta v/v$ arise. From simultaneous measurements of Γ and $\Delta v/v$ one can determine the complex ac conductance of the 2D structure, $\sigma^{AC} = \sigma_1(\omega) - i\sigma_2(\omega)$ [29].

The experiments were carried out in a dilution refrigerator in magnetic field at $B \leqslant 18$ T in the temperature interval of 20–300 mK. At the base temperature of 20 mK the magnetic field dependences of Γ and $\Delta v/v$ at various SAW intensities were recorded. The SAW frequency was changed from 28 to 307 MHz. The measurements in magnetic fields $B < 2$ T were done at a slow ramping of 0.05 T/min. A Hall probe was used to measure the magnetic field strength precisely.

III. EXPERIMENT RESULTS AND DISCUSSION

Figure 1 shows the magnetic field dependence of the real part of the ac conductance σ_1 at different temperatures at $f \equiv \omega/2\pi = 85$ MHz. It shows rich oscillation patterns corresponding not only to the integer quantum Hall effect (QHE) but also to fractional QHE regimes, which is typical for a high-quality sample.

At low field, $B < 2$ T, conductance oscillations undergo beating induced by the spin-orbit interaction [18–23]. In this paper we focus on the analysis of this effect and demonstrate only the real part of the ac conductance σ_1 because in this magnetic field $\sigma_2 \ll \sigma_1$.

For this purpose we constructed a dependence of the normalized oscillating part of the conductance $\delta\sigma_1^N = (\sigma_1 - \sigma_1^{nonosc})/\sigma_1^{nonosc}$ on the reversed magnetic field $1/B$, where σ_1^{nonosc} is the monotonically varying nonoscillating background. σ_1^{nonosc} was determined as the average value of the oscillation envelope in the way illustrated in the inset of Fig. 1. The results of such constructions at various temperatures from 20 to 300 mK are presented in Fig. 2(a). The dependences $\delta\sigma_1^N$ at $T = 20$ mK related to several SAW intensities are plotted in Fig. 2(b), where the intensity of the SAW electric field introduced into the sample ranges from 6×10^{-10} to 1.9×10^{-6} W/cm.

As seen in Fig. 2, the conductance undergoes beating, with characteristic nodes marked by arrows. The pattern of beating and nodes is much more pronounced in the dependences $\delta\sigma_1^N(B)$ acquired at different SAW intensities [Fig. 2(b)], rather than at different temperatures [Fig. 2(a)]. This is due to the small value of the signal-to-noise ratio at the minimum SAW power, at which our study of the influence of temperature on the conductivity was carried out. With an increase in the SAW intensity, the signal-to-noise ratio in the measurements of Γ and $\Delta v/v$ increases, but at the same time high intensity can set the system in a nonlinear regime. To check the signal linearity, we plot the dependence of the conductance σ_1 in a magnetic field of 0.3 T on the SAW intensity at $T = 20$ mK [see Fig. 3(a)] and on temperature at the

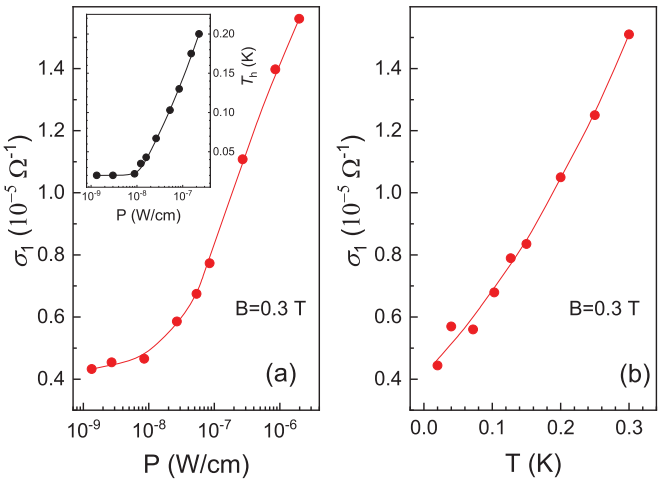

FIG. 3. Dependences of σ_1 on the SAW power P at (a) $T =$ 20 mK and (b) the sample temperature T at minimal SAW power, both at $B = 0.3$ T. $f = 85$ MHz. Inset: Dependence of the hole temperature T_h on the SAW intensity. Lines are guides to the eye.

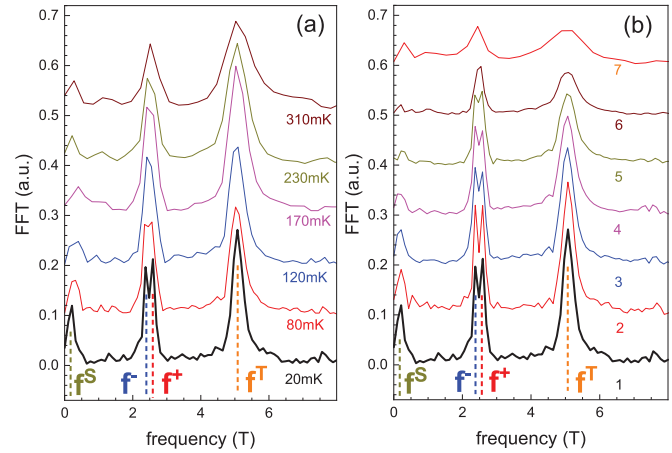

FIG. 4. The Fourier spectrum of the oscillations in the range $B < 2$ T (a) for different temperatures in the linear regime and (b) for various SAW intensities at $T = 20$ mK: (1) 6×10^{-10} W/cm, (2) 1.9×10^{-9} W/cm, (3) 6×10^{-9} W/cm, (4) 1.9×10^{-8} W/cm, (5) 6×10^{-8} W/cm, (6) 1.9×10^{-7} W/cm, and (7) 1.9×10^{-6} W/cm. Traces are offset vertically for clarity.

minimal intensity [see Fig. 3(b)]. Figure 3 evidences that the dependences $\sigma_1(T)$ and $\sigma_1(P)$ are similar. Such similarity is typical for the heating of current carriers by the SAW electric field. By comparing $\sigma_1(T)$ and $\sigma_1(P)$, the dependence of the hole temperature T_h on the SAW intensity was determined and is shown in the inset of Fig. 3(a). It can be seen from Fig. 3(a) that at $P \leqslant 10^{-8}$ W/cm the system is still in the linear regime, i.e., curves 1, 2, and 3 in Fig. 2(b) correspond to $T_h = 20$ mK. However, for curve 4 T_h is equal to 40 mK, for curve 5 $T_h =$ 107 mK, for curve 6 $T_h = 185$ mK, and for curve 7 T_h exceeds 300 mK. The values of T_h are shown for each of the curves in Fig. 2(b).

To clarify the beating structure we carried out the fast Fourier transform (FFT) procedure over the experimental data.

Figure 4 shows the Fourier spectra of the conductance for magnetic field $B < 2$ T for different temperatures in linear regime [Fig. 4(a)] and for various SAW electric field intensities at 20 mK [Fig. 4(b)]. The Fourier spectra exhibit several components. We see clearly, especially at low temperatures, a split FFT peak with the FFT frequencies $f^- \cong 2.4$ T and $f^+ \cong 2.6$ T, resulting in the appearance of both the slow oscillation FFT peak at $f^S \cong 0.2$ T and the sum FFT peak at $f^T \cong$ 5 T. The frequencies can be converted into the densities of the lower and higher populated subbands: $p^- \cong 5.8\times10^{10}$ cm^{-2} and $p^+ \cong 6.3\times10^{10}$ cm^{-2}, respectively. Therefore, $\Delta p \equiv p^S = p^+ - p^- \cong 5\times10^9$ cm^{-2}, and $\Delta p/(p^+ + p^-) \approx 4\%$.

This all confirms that the slow oscillations appear due to the intersubband transitions. Moreover, this conclusion is supported by the robustness of the f^S FFT peak in the temperature and SAW power increase, even when the FFT f^+ and f^- split is not already observed.

Now we analyze the behavior of different components of the FFT spectrum of the conductance. First, we use a bandpass filter, shown in Fig. 5(a) by the olive dotted line, to isolate the slow component from fast ones. Then, applying the inverse fast Fourier transformation, we obtain the slow oscillations of the frequency f^S, which are shown in Fig. 5(b).

Second, we should isolate from each other the two fast oscillations corresponding to upper, f^+, and lower, f^-, subbands. Since f^+ and f^- are almost equal, bandpass filtering has an ambiguity when constructing the corresponding bandpass filter. That is why the direct inverse fast Fourier transformation would not be precise. Therefore, we used specially developed software provided to us by O. E. Rut. The software algorithm is described in Ref. [13]. It carries out the bandpass filtering of the *split* FFT peak with the filter shown in Fig. 5(a) as a pink dotted line. Then, the inverse fast Fourier transformation gives a sum of fast oscillations with frequencies f^+ and f^-. Finally, this sum is fitted to the sum of two Lifshitz-Kosevich [30] terms presented in Eq. (6) of Ref. [13]:

$$\delta\sigma_1^{\mathrm{N}} = \sum_{i=1}^{2} \beta_i \exp\left(-\frac{2\pi\gamma_i}{\hbar\omega_c^i}\right) D\left(X_T^i\right) \cos\left(\frac{2\pi f_i}{B} + \phi_i\right), \qquad (1)$$

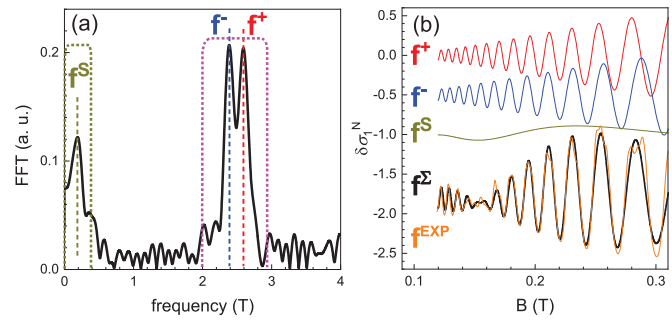

FIG. 5. (a) The Fourier spectrum of the oscillations in the range $B < 1$ T and the bandpass filters (dotted lines) used to isolate the fast and slow components. (b) The oscillating components of $\delta\sigma_1^{\mathrm{N}}$ in upper, f^+, and lower, f^-, subbands; f^S is the slow oscillation component. Also shown is the sum curve $f^\Sigma = f^+ + f^- + f^S$ (black) compared with the experimental one f^{EXP} (orange). Traces in (b) are offset vertically for clarity.

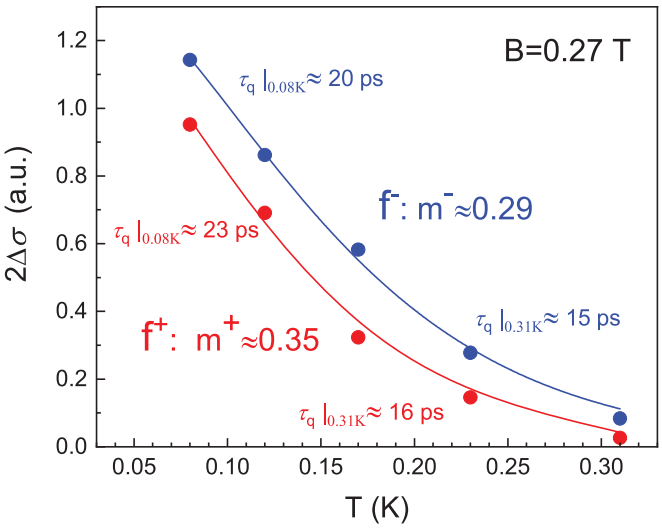

FIG. 6. The temperature dependence of $2\Delta\sigma$ for components f^+ and f^-. The solid lines are fittings using the thermal damping term of the Lifshitz-Kosevich formula.

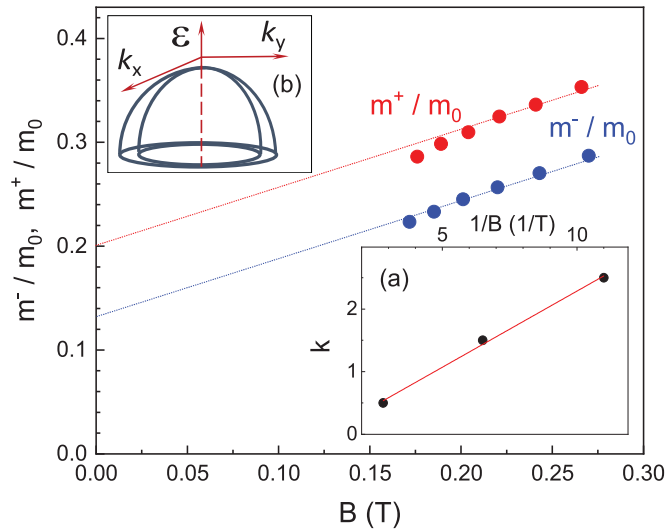

FIG. 7. The dependence of m^+/m_0 and m^-/m_0 for components f^+ and f^- on the magnetic field, $f = 30$ MHz. Lines are extrapolations of dependences $m^+/m_0(B)$ and $m^-/m_0(B)$ to $B = 0$. Inset (a): Dependence of the oscillation beating node number k on $1/B$. Inset (b): Sketch of the dispersions of holes in a 2DHG in the presence of spin-orbit interaction for the Dresselhaus mechanism.

where $D(X_T^i) = X_T^i/\sinh(X_T^i)$, $X_T^i = 2\pi^2 k_B T/\hbar\omega_c^i$. The fitting parameters $f_{1,2}$, $\gamma_{1,2}$, $\beta_{1,2}$, and $\phi_{1,2}$ are described in Ref. [13] and references therein. Fast oscillations f^+ and f^- reconstructed by using the software mentioned above are shown in Fig. 5(b). The quality of such a fitting is also illustrated by comparing the superposition curve $f^\Sigma = f^+ + f^- + f^S$ with the experimental one f^{EXP}.

Such a procedure was performed for all temperatures in the field region where beating was observed. It allowed us to build the dependences of the amplitude of oscillations on temperature in different magnetic fields.

In a 2D system with one subband the carrier effective mass m^* is usually determined from the temperature dependence of the amplitude of the SdH-type oscillations by fitting it to the factor $D(X_T)$, with the effective mass m^* being the fitting parameter.

In our case, we can independently determine m^* from temperature dependences of amplitudes as we isolate from each other the fast oscillations corresponding to upper, f^+, and lower, f^-, subbands. Figure 6 shows the dependence of the oscillation amplitudes $2\Delta\sigma$ of each component for a magnetic field of 0.27 T. Fits of the oscillation amplitudes to $D(X_T)$ provide us with m^* for each subband.

Figure 7 shows m^* values as a function of the magnetic field B for each of the spin-split subbands. m^+ and m^- increase nearly linearly with B. Linear extrapolations of the data to $B = 0$ shown by lines in Fig. 7 suggest $m^+/m_0 = 0.20 \pm 0.01$ and $m^-/m_0 = 0.12 \pm 0.01$, where m_0 is the mass of free electrons.

The quantum scattering times were also obtained from the oscillations' amplitudes: at $B = 0.27$ T the values are $\tau_q \approx 1.6\times10^{-11}$ s for the upper subband and $\tau_q \approx 1.5\times10^{-11}$ s for the lower subband at $T = 0.31$ K. The transport relaxation time $\tau_{tr} \approx 1.62\times10^{-10}$ s was found from a zero-field mobility of $\mu = 1.76\times10^6$ cm^2/V s at 0.31 K with the effective mass $m^* = (0.16 \pm 0.04)m_0$ averaged between m^+ and m^- at $B = 0$. The ratio $\tau_{tr}/\tau_q \approx 12$ indicates that a long-range scattering potential is dominant.

Magnetic field dependences of the effective mass for spin-split subbands formed as a result of the spin-orbit interaction are reported in all studies of this effect [20–23,26,27]. A possible theoretical explanation of the origin of this dependence was proposed in Ref. [31]. However, the quantum well width, as well as the sample parameters used in the calculations published in Ref. [31], differs from that studied in our work. This makes a comparison with the theory of Ref. [31] impossible.

Now, since we have estimated the values of effective masses at $B = 0$, it is possible to calculate the energy of the spin-orbit splitting Δ_{SO}. This calculation can be done by two methods.

In the first method, knowing the difference in concentrations in the subbands split by the spin-orbit interaction $\Delta p \approx p^+ - p^- \approx 5\times10^9$ cm^{-2}, we use the following formula:

$$\Delta_{SO} = \Delta p 2\pi\hbar^2/m^* = (0.16 \pm 0.04)\,\text{meV}, \qquad (2)$$

which is valid in our case since $\Delta p \ll p$.

In the second method, since it is possible to determine the magnetic field position of the oscillation beating nodes (see Fig. 3) and the modulation of the SdH-type oscillations induced by the spin-orbit interaction is realized according to the law $\sigma \propto \cos(\pi\Delta_{SO}/\hbar\omega_c)$, then $\sigma = 0$ at (in cgs units) $k = \Delta_{SO}/\hbar\omega_c = \Delta_{SO}m^*c/e\hbar B = 1/2,\ 3/2,\ 5/2$. From the slope of the dependence of k on $1/B$ shown in the inset of Fig. 7, one can determine $\Delta_{SO} = (0.2 \pm 0.05)$ meV. In both of these methods, as well as in the mobility calculations above, we used an averaged $m^* = (0.16 \pm 0.04)m_0$. As we can see, the values of Δ_{SO} determined by the different methods are close.

As mentioned in the Introduction, the scientists who studied the spin-orbit interaction in two-dimensional structures in most cases dealt either with heterostructures or with one-side-doped quantum wells. Therefore, almost all of them

observed the effect related to structural inversion asymmetry (Rashba splitting), which was much stronger than the bulk inversion asymmetry effect (Dresselhaus splitting) expected in symmetrically doped quantum wells. Also, it should be mentioned that the Dresselhaus spin-orbit interaction was studied in *n*-GaAs/AlGaAs using the weak antilocalization in the magnetoresistance effect, and the energy $\Delta_{SO} = 0.2$ meV was obtained [32]. Comparing our results with the values of the Rashba energy splitting acquired by those authors for various two-dimensional systems ($\Delta_{SO} = 30$ meV [15], 9 meV [9], 5.5 meV [11], 1.41 meV [18]), we established that theirs were significantly higher than the value obtained by us: $\Delta_{SO} = (0.16 \pm 0.04)$ meV and $\Delta_{SO} = (0.2 \pm 0.05)$ meV. Since we investigated the spin-orbit interaction in a symmetrically doped square quantum well and obtained a very small value of the spin-orbit splitting, there is a reason to believe that the origin of this effect intrinsically comes from the crystal structure of the material under study (i.e., from the absence of an inversion center), which is typical for zinc-blende ($A^{III}B^{V}$) structures (the Dresselhaus mechanism). Inset (b) in Fig. 7 shows, for simplified visualization, the hole spectrum with the presence of the Dresselhaus spin-orbit interaction mechanism. The spectrum consists of two spin subbands, giving oscillations with close frequencies, resulting in a beating.

It is worth noting that the values of the effective masses, quantum relaxation times, and energy of the spin-orbit interaction determined in the present paper do not depend on frequency in the studied range of 30–300 MHz.

In conclusion, using the high-quality structure *p*-GaAs/AlGaAs (with $p = 1.2\times10^{11}$ cm^{-2}) with a square symmetrically doped quantum well and carrying out measurements of the SdH-type oscillations in the low-temperature region, 20 mK $< T <$ 300 mK, gave us the possibility to observe, for these structures, the spin-orbit interaction which originates from the Dresselhaus effect.

ACKNOWLEDGMENTS

The authors would like to thank O. E. Rut for providing us with the FFT component separation program, G. M. Minkov for fruitful consultations, and L. E. Golub for useful discussions and careful reading of the manuscript. The authors are grateful to E. Green, P. Nowell, and L. Jiao for technical assistance. Support from the Russian Foundation for Basic Research (Project No. 19-02-00124) is gratefully acknowledged. The National High Magnetic Field Laboratory is supported by the National Science Foundation through Grant No. DMR-1644779 and the state of Florida. This research is funded in part by the Gordon and Betty Moore Foundation's EPiQS Initiative, Grant No. GBMF9615 to L.N.P., and by National Science Foundation MRSEC Grant No. DMR 1420541.

[1] G. Dresselhaus, Phys. Rev. **100**, 580 (1955).
[2] Y. A. Bychkov and E. I. Rashba, JETP Lett. **39**, 78 (1984).
[3] Y. A. Bychkov and E. I. Rashba, J. Phys. C **17**, 6039 (1984).
[4] A. C. H. Rowe, J. Nehls, R. A. Stradling, and R. S. Ferguson, Phys. Rev. B **63**, 201307(R) (2001).
[5] J. Luo, H. Munekata, F. F. Fang, and P. J. Stiles, Phys. Rev. B **38**, 10142 (1988).
[6] G. Engels, J. Lange, T. Schäpers, and H. Lüth, Phys. Rev. B **55**, R1958 (1997).
[7] V. A. Guzenko, T. Schäpers, and H. Hardtdegen, Phys. Rev. B **76**, 165301 (2007).
[8] F. Herzog, H. Hardtdegen, T. Schäpers, D. Grundler, and M. A. Wilde, New J. Phys. **19**, 103012 (2017).
[9] I. Lo, J. K. Tsai, W. J. Yao, P. C. Ho, L.-W. Tu, T. C. Chang, S. Elhamri, W. C. Mitchel, K. Y. Hsieh, J. H. Huang, H. L. Huang, and W.-C. Tsai, Phys. Rev. B **65**, 161306(R) (2002).
[10] B. Das, D. C. Miller, S. Datta, R. Reifenberger, W. P. Hong, P. K. Bhattacharya, J. Singh, and M. Jaffe, Phys. Rev. B **39**, 1411 (1989).
[11] J. Nitta, T. Akazaki, H. Takayanagi, and T. Enoki, Phys. Rev. Lett. **78**, 1335 (1997).
[12] S. I. Dorozhkin, Phys. Rev. B **41**, 3235 (1990).
[13] G. M. Minkov, O. E. Rut, A. A. Sherstobitov, S. A. Dvoretski, N. N. Mikhailov, V. A. Solov'ev, M. Y. Chernov, S. V. Ivanov, and A. V. Germanenko, Phys. Rev. B **101**, 245303 (2020).
[14] G. Minkov, V. Y. Aleshkin, O. Rut, A. Sherstobitov, A. Germanenko, S. Dvoretski, and N. Mikhailov, Physica E **110**, 95 (2019).
[15] Y. S. Gui, C. R. Becker, N. Dai, J. Liu, Z. J. Qiu, E. G. Novik, M. Schäfer, X. Z. Shu, J. H. Chu, H. Buhmann, and L. W. Molenkamp, Phys. Rev. B **70**, 115328 (2004).
[16] G. M. Minkov, A. V. Germanenko, O. E. Rut, A. A. Sherstobitov, M. O. Nestoklon, S. A. Dvoretski, and N. N. Mikhailov, Phys. Rev. B **93**, 155304 (2016).
[17] S. I. Dorozhkin, M. O. Skvortsova, A. V. Kudrin, B. N. Zvonkov, Y. A. Danilov, and O. V. Vikhrova, JETP Lett. **91**, 292 (2010).
[18] H. L. Stormer, Z. Schlesinger, A. Chang, D. C. Tsui, A. C. Gossard, and W. Wiegmann, Phys. Rev. Lett. **51**, 126 (1983).
[19] J. P. Eisenstein, H. L. Störmer, V. Narayanamurti, A. C. Gossard, and W. Wiegmann, Phys. Rev. Lett. **53**, 2579 (1984).
[20] J. P. Lu, J. B. Yau, S. P. Shukla, M. Shayegan, L. Wissinger, U. Rössler, and R. Winkler, Phys. Rev. Lett. **81**, 1282 (1998).
[21] B. Habib, E. Tutuc, S. Melinte, M. Shayegan, D. Wasserman, S. A. Lyon, and R. Winkler, Phys. Rev. B **69**, 113311 (2004).
[22] B. Habib, M. Shayegan, and R. Winkler, Semicond. Sci. Technol. **24**, 064002 (2009).
[23] Y. T. Chiu, M. Padmanabhan, T. Gokmen, J. Shabani, E. Tutuc, M. Shayegan, and R. Winkler, Phys. Rev. B **84**, 155459 (2011).
[24] M. J. Manfra, L. N. Pfeiffer, K. W. West, R. de Picciotto, and K. W. Baldwin, Appl. Phys. Lett. **86**, 162106 (2005).
[25] B. Grbić, C. Ellenberger, T. Ihn, K. Ensslin, D. Reuter, and A. D. Wieck, Appl. Phys. Lett. **85**, 2277 (2004).
[26] F. Nichele, A. N. Pal, R. Winkler, C. Gerl, W. Wegscheider, T. Ihn, and K. Ensslin, Phys. Rev. B **89**, 081306(R) (2014).
[27] V. Tarquini, T. Knighton, Z. Wu, J. Huang, L. Pfeiffer, and K. West, Appl. Phys. Lett. **104**, 092102 (2014).
[28] Z. Q. Yuan, R. R. Du, M. J. Manfra, L. N. Pfeiffer, and K. W. West, Appl. Phys. Lett. **94**, 052103 (2009).

[29] I. L. Drichko, A. M. Diakonov, I. Y. Smirnov, Y. M. Galperin, and A. I. Toropov, Phys. Rev. B **62**, 7470 (2000).

[30] I. M. Lifshits and A. M. Kosevich, Sov. Phys. JETP **2**, 636 (1956).

[31] G. E. Simion and Y. B. Lyanda-Geller, Phys. Rev. B **90**, 195410 (2014).

[32] W. Desrat, D. K. Maude, Z. R. Wasilewski, R. Airey, and G. Hill, Phys. Rev. B **74**, 193317 (2006).